Critical evaluation of procedures fundamental to reverse osmosis membrane autopsy

Thiago Ranzani da Costa[a], René Peter Schneider[b],*

[a]*Department of Microbiology, Institute of Biomedical Sciences, University of São Paulo, Av. Professor Lineu Prestes, 1374, 05508-900 São Paulo, Brazil, Tel. +55 11 3091 7343; email: thi_cos@yahoo.com.br*
[b]*Department of Chemical Engineering, Polytechnical School, University of São Paulo, Av. Prof. Luciano Gualberto, Travessa 3, n. 380. São Paulo – SP, Brazil, CEP 05508-900, Tel. +55 11 3091 2232; email: schneiderpqi@usp.br*

ABSTRACT

Membrane autopsies are destructive investigations performed to identify the cause of membrane failure or of loss of membrane performance. Procedures important for the outcome of autopsy studies were critically evaluated in this work, including foulant removal, sample drying at 100°C and loss-on-ignition at 550°C. Colorimetric assays for silica and iron in fouling samples were investigated as surrogates for field analytical procedures. Homogenization in a blender worked best for foulant removal, followed by gentle scraping, whilst sonication was ineffective. A thin fouling film was left on the membrane surface even after application of the best removal techniques. A time of 3 h was sufficient to allow for sample drying at 105°C. Loss-on-ignition at 550°C was completed after 20 min, but significant reductions of $FeCl_3$ (50%), ammonium chloride and ammonium sulfate (both 100%) demonstrate that loss-on-ignition weight loss may not be an accurate measure of organic matter content in foulant samples with a high proportion of inorganics. Calibration curves for quantification of iron and silica in kitchen blender foulant homogenates with the colorimetric phenanthroline and ammonium molybdate assays, respectively, had to be established by standard addition directly to the sample. Fouling removal with a kitchen blender produced homogeneous extracts suitable for chemical analysis with field kits.

Keywords: Reverse osmosis; Membrane fouling characterization; Membrane autopsy; Iron analysis by phenanthroline; Silica analysis by molybdate

1. Introduction

Spiral wound reverse osmosis and nanofiltration membranes, which dominate the desalination market [1], split feedwater into a low salt permeate and a high salt concentrate stream. Membrane performance in these systems is strongly affected by the accumulation of rejected feedwater components. When membrane permeability drops below a predetermined threshold because of such fouling layers, the membrane skid is temporarily taken out of production for removal of accumulated foulants by a combination of chemical dissolution and hydraulic cleaning [2]. Cleaning generally does not restore full original membrane permeation performance. Irreversible foulants not removable by the cleaning techniques accumulate progressively at the surface and eventually reduce filtration performance to the point where membrane replacement is required. Optimization of membrane cleaning protocols requires accurate identification of these irreversible foulants.

In real systems, membrane fouling is rarely caused by a single type of mechanism [3,4]. Fouling may be passive or active, depending on whether compounds incorporated into the reject layer are further modified post-deposition or not. Each feedwater component either solid or dissolved rejected

* Corresponding author.

at the membrane surface is subject to passive accumulation. Further transformation of the foulants in the reject layer will depend on their physicochemical nature. Inorganic dissolved salts may eventually reach saturation and precipitate on the membrane surface. In this case, crystallization clusters form in the fouling layer or in the concentrated feedstream and grow by incorporating individual ions into the crystal lattices, thus sequestering otherwise mobile species from the liquid into the adsorbed solid layer [5]. Particularly complex fouling mechanisms are those where polymerization is involved, such as gel formation by silicates [6], humic substances and other organic polymers. In all of the fouling mechanisms described above, the rate of accumulation of the foulants depends essentially on their rate of transport from the bulk liquid to the membrane surface.

Biological fouling, where microbial biofilms colonize the membrane surfaces, is of an entirely different nature [7]. In this instance, bacterial cells (particles) capable of metabolizing organic monomers and macromolecules from the foulant layer replicate and begin to develop a biofilm, where the cells become encased in an extracellular polymer matrix [8]. The biofilm matrix is composed of gel-forming substances excreted by biofilm cells, which act as glue and entrap ions, organic monomers and polymers, colloidal and particulate organic and inorganic feedwater components [8]. Biofilms may cover the substrata on which they grow uniformly or not, and they often contain a mix of live and dead microbial cells of a diversity of microbial species [7]. Microbial biofilms are dynamic and self-replicating foulants. Cell growth in the membrane foulant layer does not depend on the transport of additional cells to the membrane surface, but on the availability of organic and inorganic nutrients. Microbial activity modifies the chemical composition of the foulant layer. Excreted hydrolases break down macromolecules such as lipids, proteins and polysaccharides. Many of the small molecular weight organics metabolized by the cells are by themselves non-fouling, but become important foulants once incorporated into biomass. In reverse osmosis systems, operational impacts of biofouling include flux decline, increased salt passage and pressure drop inside the feed flow channel [9].

Membrane autopsies are destructive investigations performed to identify the cause of membrane failure or of the loss of membrane performance [10]. Autopsy begins with the removal of the membrane from the pressure vessel and its transfer to the autopsy laboratory. Speedy delivery is essential because it is not possible to cool the elements during transport as it is a standard practice for biological or chemical sampling to halt or reduce biological activity to a minimum. Once in the lab, the element should be ideally subjected to a wet performance test under standard conditions similar to those used to define its performance when new. Next, the intact element is visually inspected for signs of damage or of biogrowth, which may include visible protrusion of fungal colonies or of bacterial slimes from the feed channel or pressure marks from the antitelescoping device on the membrane roll at the element outlet. The element is then cut open and membrane leaves are carefully unrolled on a table and inspected for signs of damage on glue lines or membrane surfaces. Special attention is given to assessment

of the visible fouling deposits, if present. Properties such as thickness, consistency (sliminess), color, homogeneity or unevenness of distribution will determine the locations of deposit sampling.

The foulant layer may be analyzed non-destructively by a range of microscopy procedures [11] or chemical analysis techniques [12]. The most commonly employed microscopic technique is scanning electron microscopy coupled to EDS element analyzers. This combination of techniques allows high-resolution morphological investigation of the foulant layer as well as limited qualitative elemental composition characterization. Small membrane samples are cut carefully from the membrane leaf, subsequently dried in air or by chemical dehydration and then sputter-coated in order to increase contrast. Major drawbacks of this technique include (i) the need to dehydrate the samples, a particularly troublesome procedure for biological or other hydrated organic and inorganic constituents [13], (ii) the high vacuum environment that produces a hydrophobic interface as opposed to the hydrophilic interface; the samples are exposed to when wet, and (iii) the limited depth of penetration of EDS spectroscopy restricted to the top 1–2 μm of the sample, which may severely limit the information about the composition of deeper foulant layers. Contact angle analysis is sometimes employed for surface free energy and hydrophobicity analysis of foulant surfaces [13]. Diagnostic liquids other than water used for surface free energy investigation may introduce serious sample artefacts into the foulant layer interface [14]. Other non-destructive techniques include atomic force microscopy [15] for surface topography characterization and Fourier transform infrared spectroscopy in the attenuated reflectance mode for chemical analysis [16].

Most chemical or biological characterization methods require recovery of the foulants from the membrane surface for further analysis. Such removal needs to be complete in order to obtain relevant autopsy characterization data, but a systematic comparison of the efficiency of different removal procedures is lacking. A search in the Scopus database using the search terms "reverse osmosis autopsy" produced 210 references published since 2013. 25 of these articles from leading peer-reviewed journals described membrane autopsies of elements retrieved from commercial plants. Examination of the foulant removal procedures employed in these studies revealed a preference for scraping (10 hits), followed by sonication (7 hits), extraction/desorption (4 hits) and vortex agitation alone (1 hit). In three articles, the method of removal of foulants was not specified. In wet extraction, the fouled membrane is immersed in solutions designed to solubilize specific foulants of interest, such as silica [17] or organic as well as inorganic foulants [18]. Both scraping and sonication may potentially damage the membrane surface. In this work, the efficiency of foulant removal by these two methods was compared with homogenization with a blender as proposed by Donegan et al. [19] to remove bacteria from biofilms without damaging the cells. The latter method has never been evaluated for membrane fouling studies. Many analytical methods require foulant samples to be dried at 100°C prior to analysis. In some cases, the materials are subjected to loss-on-ignition at 550°C for determination of organic matter content. We

also investigated whether inorganic salts potentially present in reverse osmosis fouling layers may be lost during these thermal pretreatments. Membrane autopsies for RO elements from plants located far from the service providers tend to be logistically complex, expensive and with lengthy turnaround times since membrane elements have to be preserved, packed and frequently shipped by air to be examined by autopsy service providers. In these instances, it would be helpful if critical foulants could be analyzed directly in the field. Such analyses require knowledge of potential sample matrix effects on analysis results and, if detected, procedures to minimize the impact of these interferences. Colorimetric assays for silica and iron in fouling samples as surrogates for field colorimetric analytical procedures were evaluated for matrix interference.

2. Materials and methods

All chemical standards used were of analytical grade. Ultrapure water was obtained from an USF ELGA purificator, model UHQ-PS (England).

2.1. Preparation of artificially fouled membranes

Twenty-five samples (33.6 cm²) were cut from membranes removed from a new RO element (Model No: RE-70-1812, CSM, Korea) for growing biofilms. Five samples were separated to obtain clean membrane weight loss data. The remaining 20 samples used for growing biofilms were attached at the permeate side down with an insulating tape to an impermeable plastic support in order to restrict biofilm growth to the polyamide-coated separation layer. The samples were exposed for 3 months to flowing water pumped from the rowing channel of the University of São Paulo for the formation of fouling layers.

2.2. Fouling removal methods

Scraping, sonication and shredding were evaluated for removal of fouling layers from membranes. Each method was analyzed in triplicate with samples of artificially biofouled membranes. Scraping was performed by gentle movements of a sterile spatula in order to prevent mechanical damage of the membrane surface. For sonication, membrane samples (33.6 cm²) were placed inside a glass beaker filled with distilled water degassed for 10 min prior to membrane immersion, and treated for 5 min at maximum power (Ultrasonik TM sonicator, Santa Clara, CA). Shredding of fouled membranes was performed for 2 min at maximum power in a kitchen blender in 200 mL of sterile ultrapure water (~200 mL), the minimum volume required to completely cover the cutting blades. The blender jar and cutting assembly were disinfected with 70% ethanol prior to the treatment.

Clean and fouled membranes, or, where applicable, the combined fragments of a shredded membrane, were dried for 12 h at 70°C (higher temperatures caused membrane damage, not shown) to determine dry weight. The amount of foulants on the membrane surfaces was calculated from the weight difference of the dry fouled and the dry clean membrane. The efficiency of foulant layer removal was quantified according to Eq. (1) below:

$$\text{Efficiency of foulant removal} = \left(\frac{\text{Dry weight after foulant removal}}{\text{Dry weight before foulant removal}} \right) \times 100\%$$

2.3. Total solids and volatile solids analysis

Porcelain crucibles used in the analysis of total and volatile solids were manipulated with steel pincers. The crucibles were washed with 4% Extran, rinsed thoroughly with ultra pure water, heated for 15 min in a muffle furnace at 550°C, cooled to room temperature in a desiccator and weighed on an analytical balance. The procedure was repeated until crucible weight stabilized. Crucibles with samples for the determination of total solids were dried at 105°C for an initial period of 1 h, then cooled in a desiccator for 15 min and weighed. This procedure was repeated until dry weight stabilized. The samples were then transferred into a muffle furnace for varying periods of time for volatilization of solids at 550°C. After cooling in a desiccator, the samples were weighed and the procedure was repeated until the weight was stabilized. Silica (Na_2SiO_3), ferrous sulfate ($FeSO_4 \cdot 7H_2O$), strontium sulfate ($SrSO_4$), calcium sulfate ($CaSO_4 \cdot 2H_2O$), barium sulfate ($BaSO_4$), calcium carbonate ($CaCO_3$), ammonium chloride (NH_4Cl), sodium hydroxide ($NaOH$), calcium phosphate ($Ca_3(PO_4)_2 \cdot 2H_2O$), ferric chloride ($FeCl_3$), aluminum sulfate ($Al_2(SO_4)_3$), ferrous sulfide (FeS) and ammonium sulfate ($(NH_4)_2SO_4$) were also tested by loss-on-ignition to investigate whether compounds other than carbon could be volatilized from the sample during treatment. The compounds were dried in an oven for 12 h before loss-on-ignition. Each sample was analyzed in triplicate.

2.4. Colorimetric analysis of biofilm constituents

Samples of six fouled RO elements with an area of 289 cm² were disaggregated in a blender (Black & Decker IB900, Uberaba, Brazil) with 200 mL of ultrapure water at maximum speed for 2 min. Membrane fragments were removed with a sieve and the filtrate was used in the analyses. To check for matrix effects, quantification with an external standard curve was compared with quantification by standard addition of calibration standards to the samples [20]. All samples were analyzed in triplicate.

Silica was quantified by the ammonium molybdate method [21]. Briefly, 5 mL of sample were mixed with 200 mg of sodium bicarbonate and 45 mL of ultrapure water in a platinum capsule. The solution was digested in a steam bath for 1 h. After cooling, 2.4 mL of 0.5 M sulfuric acid were added under constant stirring. The solution was transferred to a Nessler tube, made up to 50 mL with ultrapure water and 1 mL hydrochloric acid (concentrated HCl diluted 1:1 with ultrapure water) and 2 mL 10% (w/v) ammonium molybdate were added. The solution was mixed and incubated for 7 min

before addition of 1.5 mL of 10% (w/v) oxalic acid followed by homogenization. Absorbance was measured at 410 nm after 2 min. For calibration, a stock solution of 4.73 g L^{-1} Na$_2$SiO$_3$x9H$_2$O was diluted to produce solutions containing 0.2, 0.8, 2, 5 and 10 mg SiL^{-1}. 50 mL of calibration solution were digested prior to colorimetric analysis with 200 mg of NaHCO$_3$ as described earlier.

Total iron was analyzed by the phenanthroline method [21]. Briefly, 5 mL of sample, 0.2 mL HCl and 0.1 mL 10%(w/v) hydroxylamine were thoroughly mixed. After incubating for 10 min, 1 mL of ammonium acetate buffer (250 g NH$_4$C$_2$H$_3$O$_2$ dissolved in 150 mL ultrapure water mixed with 700 mL glacial acetic acid) and 0.4 mL of 1 mg mL^{-1} phenanthroline were added, the solution was made up to 100 mL with ultrapure water and then incubated for 10 min for color development. Absorbance of the complex was measured at 510 nm with a spectrophotometer. Calibration was performed in the concentration range of 0.1, 0.2, 0.4, 0.6 and 1 mg FeL^{-1} with suitable dilutions of a 2 mg L^{-1} Fe stock solution, prepared with FeCl$_3$.

2.5. Scanning electron microscopy

Scanning electron microscopic examination of membrane surfaces metalized with platinum was performed on a FEI Quanta 600 FEG (Hillsboro, Oregon, USA) equipment.

2.6. Statistical analysis

Non-calibration data were first assessed for statistical significance of the difference of means by a one way ANOVA test ($p = 0.05$). If the hypothesis of similarity of means was rejected, a Tukey test ($p = 0.05$) was performed next to identify the means that differed from each other.

Statistical evaluation of calibration data was performed for both the raw dataset, which includes all replicates of calibration points, and data averaged for each point. Calibration data were first submitted to a Grubbs test ($p = 0.05$) to detect outliers, but none were found. Normality distribution of data was evaluated with a Shapiro–Wilk test ($p = 0.05$). Data from individual calibrations and, when comparing two different calibration curves, the combined datasets, were checked for heteroscedasticity with a White test ($p = 0.05$). Calibration curves were constructed using the standard inbuilt excel calculation routine that incorporates an ANOVA analysis. A Student t-test ($p = 0.05$) using the excel slopes test analysis routine of Zaiontz [22] was used for comparison of slopes of external and standard addition calibrations. Since there may be instances where the use of Student t-test for comparison of slopes may not be appropriate, such as when data distribution does not follow normality or when only a small calibration dataset is available [23], an alternative slope comparison procedure based on wild bootstrap methods proposed by Estévez-Péres et al. [24] was carried out with the program routine implemented in R-statistics software [25].

3. Results and discussion

3.1. Foulant removal from membranes

The experiments to test the efficiency of foulant removal procedures had to be performed with artificially fouled membranes because of the need to compare weights of clean membranes with those of fouled ones. RO membranes obtained from a new element were exposed in laminar fluid flow cells to water from the rowing channel of the University of São Paulo for establishment of a fouling layer. After 3 months, the membrane side exposed to the raw water was covered with a thick fouling film, whilst the backside remained clean (not shown). The membranes were divided into batches of five for testing the efficiency of fouling removal techniques. Sonication reduced the amount of foulants by only 25% (Fig. 1). Scraping with gentle spatula movements and shredding in a blender were more efficient and removed 79% and 90% of the deposits, respectively (Fig. 1). Gentle surface scraping is the method recommended for foulant removal from membrane surfaces in several published autopsy protocols [10,26]. The disadvantage of this technique is the need to limit the force applied on the scraping tool to avoid damage to the thin polyamide separation layer, which may compromise the efficiency of this procedure for removal of the material closest to the membrane. A second disadvantage of the scraping method is the potential variability of efficiency between operators. Removal of membrane foulants with a kitchen blender not only benefits from the stronger shear forces that produce more consistent surface cleaning, but it also produces a homogenized solution suitable for further chemical or biochemical analysis of foulant constituents. Mixing in a kitchen blender does not harm microorganisms, the better sample dispersion achieved with this technique might increase bacterial recovery from samples [27]. Performing foulant removal with a machine (blender) instead of a human operator (scraping) allows for better standardization of the procedure. The blender, however, is not adequate for obtaining foulant samples for dry weight or loss-on-ignition determinations.

The low efficiency of fouling removal by sonication was surprising, since the sonication protocol used here was successfully employed in previous work for removal of pure culture *Pseudomonas aeruginosa* biofilms from solid surfaces [28] and this method has been employed by other researchers in membrane surface cleaning studies [18,29]. In sonication, substantial amounts of mechanical power are transmitted by small vibratory movements between 20 and 500 kHz to the liquid [30,31]. The vibrations in the liquid cause gas nuclei to expand during the expansion cycle of the acoustic wave absorbing dissolved gases and vapors. In the compression cycle, part of the gases incorporated into
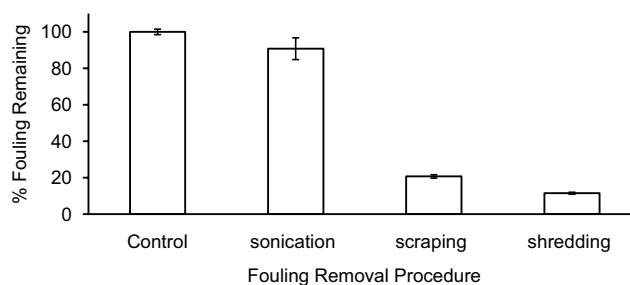

Fig. 1. Removal of foulants from reverse osmosis membranes exposed in laminar flow cell for 3 months to flowing water pumped from a surface pond at the University of São Paulo.

the bubble is expelled again only for the bubble to grow and incorporate new volatile molecules in the next expansion cycle. Eventually the bubbles reach a size where they suffer catastrophic collapse by cavitation producing local hot spots with temperatures and pressures of up to 4,000 K and 100–200 MPa, respectively [30]. Bubble diameter at cavitation collapse is usually several microns, but bubbles may grow up to 200 µm prior to collapse. Bubble collapse will occur a short distance away from the substratum producing a jet of liquid with speeds of up to 110 m/s directed at the surface, which shears away fouling deposits. Additional surface cleaning is contributed by bubble pulsation-induced small-scale liquid movements and microstreaming, where the bubbles travel on the fouled surface along paths in direction of nodes, with strong shear forces produced at the gas/foulant interface [32]. Material removal may be enhanced by acoustic streaming, acoustically-induced macroscopic currents at the scale of centimeters. Ultrasonic cleaning relies on this combination of macro- and microcleaning mechanisms for material removal and is ultrasound frequency dependent. High frequencies tend to produce small bubbles less capable of dislocating the fouling layers from the membrane surface. Several authors investigated the use of ultrasound to control fouling deposit formation during membrane filtration [33–36] with clear beneficial effects on flux maintenance. However, attempts to apply sonication to the cleaning of NF or RO membranes were less successful. Ultrasound in clean water did not result in good cleaning [37–39], in fact, membrane permeability was reduced after ultrasonic cleaning [39]. Ultrasound energy must be very well controlled to avoid physical damage of membrane surfaces [37,38]. Ultrasound cleaning was only effective when combined with chemical cleaning agents, a procedure not acceptable in membrane autopsy [37–39], where the chemical constitution of the sample must be preserved. Cavitation bubble collapse produces high energy liquid jets that may mechanically damage the membrane surface [40] and contaminate the foulant sample with membrane surface particles [37,38]. The high temperatures produced during cavitation collapse likely stimulate chemical reactions of organics and inorganics in the affected area. Some of the chemicals produced during bubble collapse are toxic to microbes and might thus affect cell viability and/or composition data [41]. Sonication, therefore, should not be used for removing foulants in membrane autopsy.

None of the removal methods restored the membranes to their original clean condition (Fig. 2g). The smoother surface texture of membranes that had their foulant layer removed by either scraping (Fig. 2b) or shredding (Fig. 2f) compared with the surface roughness of the clean membrane (Fig. 2c) suggests that a tightly attached thin fouling layer remained on these surfaces after cleaning. The nature of these foulants is not known, but due to their location, further studies should be undertaken to chemically characterize these substances. They may be more critical for loss of membrane performance than the much larger quantity of material easily removed from the foulant layer by scraping or blender treatment. There are many reports about lateral variability of foulants on membrane surfaces, but depth profiling studies of foulant layers are rare. The challenge in depth profiling analysis is the minimization of disturbances from layers outside the zone of interest that may compromise the relevance of the

results. The resolution has to be appropriate for the generation of meaningful vertical molecular or elemental distribution data. One of the simplest true depth profiling techniques capable of undisturbed sample characterization is confocal scanning laser microscopy. This technique widely used in the study of microbial biofilms [42] can also be applied to analyze the vertical distribution of molecules in fouling layers, provided they harbor chemical groups that can be excited by the instrument laser beam [43,44]. Other more sophisticated physical depth profiling techniques such as positron annihilation lifetime spectroscopy [45,46] or Rutherford backscattering spectrometry [47], whilst providing adequate vertical resolution suffer from the disadvantage of the samples having to be analyzed in high vacuum environments, which causes significant modifications to the structures of hydrated polymers in the foulant matrix [13,48].

3.2. Drying at 105°C

Sample drying is one of the critical steps in the determination of total solids. Water loss from the membrane foulants removed from commercially operated reverse osmosis membranes occurred gradually and was complete after 3 h (Fig. 3a). Water distribution in membrane fouling samples depends strongly on their composition [49]. In fresh samples, most water will be located in the surface film and in the pores, its movement will only be marginally constrained by physicochemical interactions. Adsorbed water is retained by physicochemical interactions, mainly Van der Waals interactions, on the surfaces of materials. Its removal depends on the temperature and humidity of the environment and will not lead to modifications of material structure. Water incorporated into the structure of materials, for example, crystal water either physically trapped inside crystalline solids or that is part of the crystal structure of such solids is not readily lost upon drying. These types of water predominate when membrane foulants are made up primarily by inorganic deposits. In samples with a significant contribution of hydrated organic and inorganic matter, such as hydrogels of chemical or biological origin, including microbial biofilms with their extracellular matrices, a significant proportion of water, up to 20% of total weight, will be immobilized in flexible organic matter, where it is actively involved in the definition of spatial structure. This type of water is commonly associated with biological samples and it is of fundamental importance to the stabilization of the extracellular matrix of microbial biofilms [8]. Its removal will cause structural modification of the organic molecules it is associated with [13,50,51]. When a sample is exposed to 105°C in a dry atmosphere, the first water to be lost is water from the surface film and free pore water, followed by interstitial adsorbed and absorbed water, depending on sample constitution. The resistance to movement of the different types of water in the sample produces distinctive sections in sample dehydration profiles [52]. To investigate whether the water loss behavior observed for the organically fouled membrane samples was typical for environmental biofilms, activated sludge and biodigestor biomass from a reactor treating activated sludge solids were included in the study. Interestingly, water loss was slower for activated sludge flocs, where sample weight remained stable for the first two
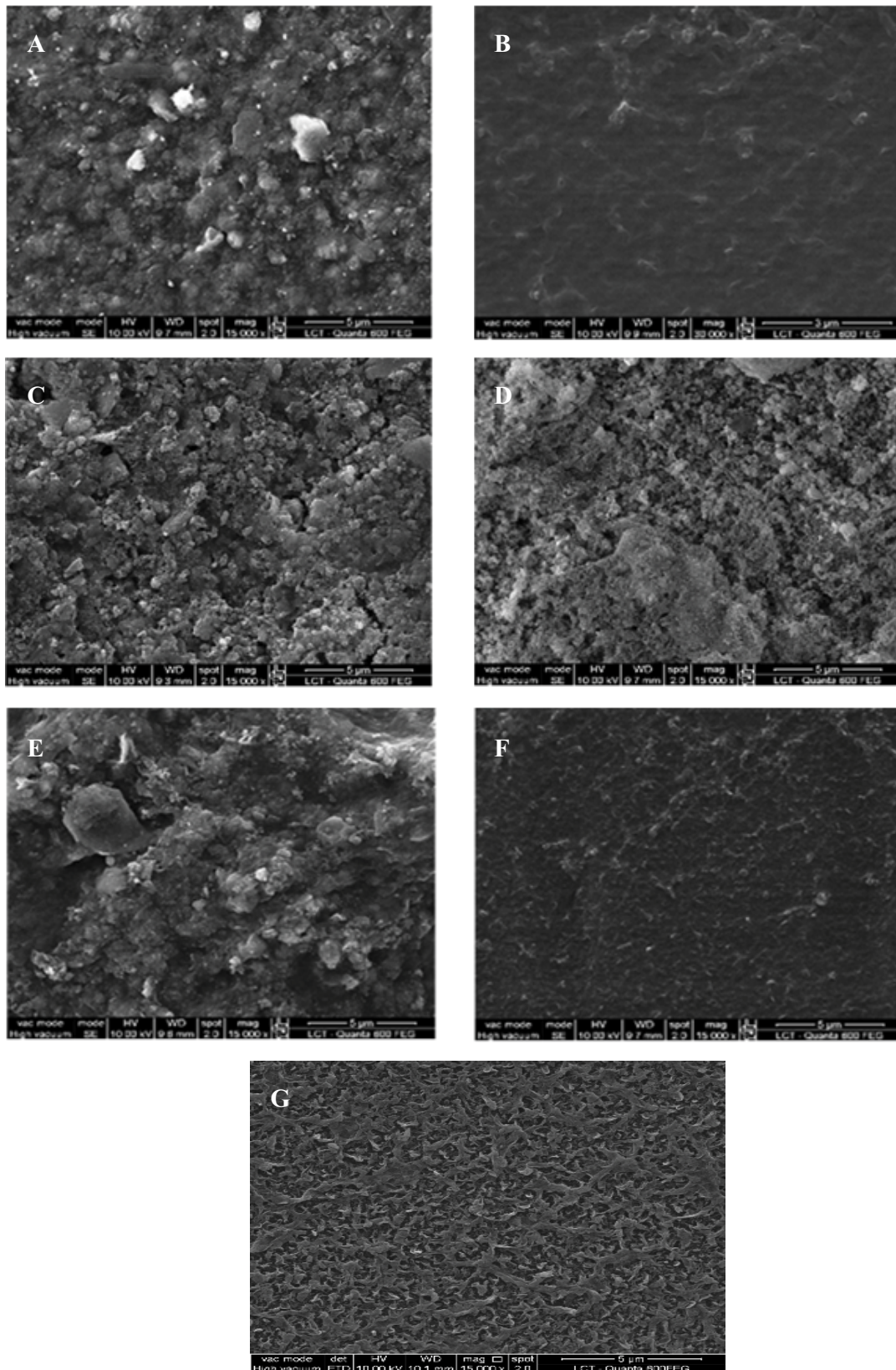
Fig. 2. Scanning electron micrographs membrane samples before (A, C, and E) and after foulant removal (B, D and F). Clean membrane for comparison (G). Removal method: scraping (A, B), sonication (C, D) and shredding (E, F). Please note the rough surface of the clean membrane and the comparatively smooth surfaces of the membranes cleaned by scraping (B) or shredding (F).
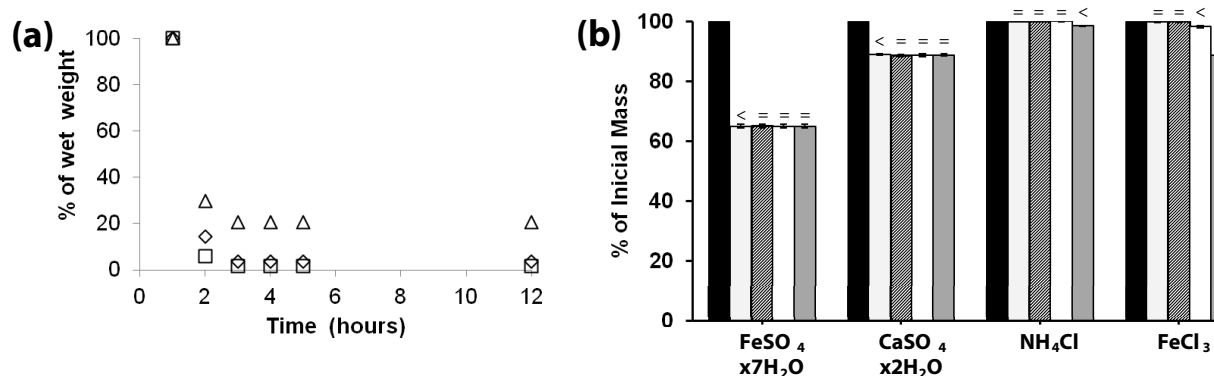
Fig. 3. Effect of drying at 105°C on dry weight of foulants. (a): fouling layers removed from reverse osmosis membranes 1 (triangles), 2 (rhombus) and 3 (squares). Results of triplicate analyses of each sample. Error bars (not shown) were smaller than the thickness of the line on the bar graph or of the dots in the figure. (b): Weight loss of pure model inorganic compounds after 0 h (black bar), 1 h (light gray bar), 2 h (pattern fill), 3 h (white bars) and 12 h (dark gray bar). Tukey test ($p = 0.05$) comparison of adjacent bars: <: average value shown in the bar significantly smaller than that of the preceding one; =: average value shown in the bar equal to that of the preceding one. No weight loss was detected for salts of silica, strontium sulfate, barium sulfate, calcium carbonate, sodium hydroxide, calcium phosphate, aluminum sulfate, ferrous sulfide and ammonium sulfate.

hours and dropped suddenly from the second to the third hour of incubation (not shown). In biodigestor suspended biofilm samples, the bulk of the water was removed from the first to the second hour (not shown). For all biofilm samples, however, dry weight was stabilized after 3 h, indicating this to be the recommended drying time.

Weight loss of selected pure inorganic compounds potentially present in membrane fouling layers was also investigated. During the 12 h drying at 105°C, the hydrated compounds ferrous sulfate and calcium sulfate showed the largest weight loss of 38% and 15%, respectively (Fig. 3b). These values were slightly smaller than the calculated water content of these salts of 45.5% and 21%, respectively, suggesting that hydration water removal was not complete after drying at 105°C. Smaller overall weight losses of 12.4% and 1.7% in 12 h were recorded for ferric chloride and ammonium chloride (Fig. 3b). Weight loss for both sulfate salts was completed after 1 h. The weight of iron chloride remained steady for the first two hours, and a small but significant weight loss of 2% was recorded at the third hour mark, with a further 10.4% of weight reduction over the next 9 h. Ammonium chloride weight remained steady for 3 h, and a small loss was recorded after 12 h only. No weight loss was detected for salts of silica, strontium sulfate, barium sulfate, calcium carbonate, sodium hydroxide, calcium phosphate, aluminum sulfate, ferrous sulfide and ammonium sulfate. There was no change to dry weight for samples kept for up to 1 h in the desiccator (not shown).

3.3. Loss-on-ignition at 550°C

Loss-on-ignition at 550°C in a muffle oven of samples dried in the previous section was complete after 20 min for most membrane foulants and pure salts (Fig. 4). Loss-on-ignition of the pure inorganic compounds tested in the drying experiment varied depending on compound nature. The small weight loss of dried ferrous sulfate-heptahydrate (15%), calcium sulfate dihydrate (8%), sodium hydroxide (10%) and calcium phosphate dihydrate (12%)

at 550°C probably occurred due to release of tightly bound residual water that remained in the sample after drying at 105°C, since these compounds were hygroscopic and have high boiling temperatures of 1,312°C, 1,400°C, 1,388°C and 1,391°C, respectively [53]. The weight loss of ferric chloride ($FeCl_3$) of approximately 50% was due to decomposition at temperatures above its boiling point of 280°C when it spontaneously disproportionated to $FeCl_2 + Cl_2$, resulting in the loss of mass due to emission of chlorine gas [53]. Both ammonium salts were volatilized completely at 550°C. Ammonium chloride begins to sublimate at a temperature of 200°C, reaching maximum sublimation rates at 345°C, when the salt is converted into gaseous ammonia and hydrochloric acid [54]. Ammonium sulfate begins to decompose at a temperature above 250°C, first into ammonia and ammonium hydrogen sulfate. The latter decomposes at 450°C into volatile ammonia and sulfuric acid [54]. Iron sulfide did not undergo weight loss under the conditions tested. Clearly, loss-on-ignition weight loss may not be an accurate measure of organic matter content of a membrane foulant sample particularly in reverse osmosis or nanofiltration where significant proportions of inorganics may be incorporated into the fouling layer. Residual structural water not removed in the drying stage may also contribute to weight reduction in loss-on-ignition. It is, therefore, recommended to employ TOC analysis for quantitation of organic carbon in such samples.

3.4. Calibration curves for colorimetric and titration assays

The application of colorimetric and titrimetric methods for chemical characterization of the supernatant recovered after shredding of fouled membranes was evaluated using analysis of silica and total iron as model compounds. Fouled membrane samples in these experiments were obtained from commercially operated plants. Wet chemistry analytics generally rely on external calibration curves established using standards of the target analytes diluted in ultrapure water for quantification. Because of the high likelihood of the occurrence of interfering substances in samples from fouled membranes,

an alternative approach of calibration by standards addition directly to the sample matrix was also evaluated. Statistical analysis of external and standard addition calibration data is summarized in Tables 1 and 2 for iron and silica quantitation, respectively. The Grubbs test ($p = 0.05$) performed first did not uncover outliers in the entire calibration dataset. The Shapiro–Wilk test indicated that all calibration data were normally distributed ($p > 0.05$). All calibration curves were
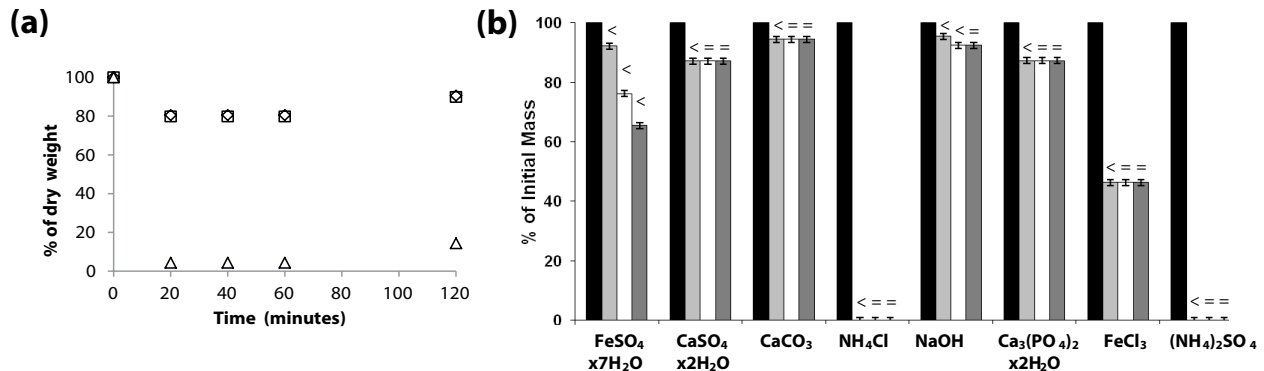

Fig. 4. Weight loss after calcination at 550°C. (a): fouling layers removed from reverse osmosis membranes 1 (triangles), 2 (rhombus) and 3 (squares). Results of triplicate analyses of each sample. Error bars (not shown) were smaller than the thickness of the line on the bar graph or of the dots in the figure. Exposure times in the oven: 0 h (black bar), 20 min (light gray bar), 1 h (white bar), 2 h (dark gray bar). Tukey test ($p = 0.05$) comparison of adjacent bars: <: average value shown in the bar significantly smaller than that of the preceding one; =: average value shown in the bar equal to that of the preceding one. No weight loss was detected for salts of silica, strontium sulfate, barium sulfate, aluminum sulfate and ferrous sulfide.

Table 1
Test statistics for colorimetric iron analysis in different calibration matrices. S: external standard curve, M1 to M5: standard addition to membrane fouling extracts from five membrane samples with different foulant characteristics. Raw data: all calibration measurements (triplicates per concentration) were considered in the analysis. Means: only the mean values were considered for each calibration point (1 point per concentration)

(a)   Values of statistical parameters of individual regression lines

Dataset	Statistical test	Calibration matrix					
		S	M1	M2	M3	M4	M5
Raw	Outlier detected in Grubbs test	None	None	None	None	None	None
	Shapiro–Wilk p	0.45	0.16	0.28	0.22	0.12	0.20
	White p	0.90	0.21	0.57	0.23	0.59	0.18
	R^2	0.99	0.98	0.99	0.98	0.99	1.00
	Regression p	1.2×10^{-10}	3.2×10^{-9}	3.8×10^{-11}	1.3×10^{-9}	4.4×10^{-10}	9.7×10^{-12}
Means	Outlier detected in Grubbs test	None	None	None	None	None	None
	Shapiro–Wilk	0.77	0.46	0.63	0.46	0.38	0.47
	R^2	1.00	0.99	0.99	0.99	0.99	1.00
	Regression p	1.2×10^{-5}	6.5×10^{-5}	1.2×10^{-5}	4.9×10^{-5}	2.5×10^{-5}	6.2×10^{-6}

(b)   Pairwise analysis of slopes of calibration lines. S: external standard curve, M1 to M5: standard addition to membrane fouling extracts from five membrane samples with different foulant characteristics. Student t analysis performed with unspooled standard error. WGhs: within groups heteroscedasticity by the Breusch–Pagan test; BGhs: between groups heteroscedasticity by the Breusch–Pagan test

Dataset	Test Parameter	S/M1	S/M2	S/M3	S/M4	S/M5
Raw	Student t p	1.0×10^{-11}	1.6×10^{-15}	1.3×10^{-9}	1.8×10^{-11}	1.4×10^{-16}
	WB	0	0	0	0	0
	WGhs	0.15	0.86	0.47	0.93	0.90
	BGhs	0.00	0.01	0.02	0.01	0.01
Means	Student t p	2.6×10^{-6}	8.0×10^{-8}	3.1×10^{-5}	3.3×10^{-6}	2.5×10^{-8}

WB Breusch–Pagan 1: Within-groups heteroscedasticity.
WB Breusch–Pagan 2: Between-groups heteroscedasticity.

linear (Fig. 5) and coefficients of determination were 99% or higher, except for iron in matrix M3 and calibration with raw data, where R^2 was 98%. ANOVA significance p values of the linear calibrations were also well below 0.05 in all instances indicating each calibration point was statistically different from the others in the series. Residuals plots for raw calibration data were mostly randomly scattered around 0 (Figs. S1–S4). The White test revealed that individual calibration data were homoscedastic, for example, that the standard errors of the regression were normally distributed over the entire concentration interval.

Comparison of standard addition and external calibration curves by both the Student t and bootstrap tests demonstrated statistically significant differences of slopes, which suggests pronounced matrix interference in iron analysis (Table 1). This outcome was confirmed by heteroscedasticity analysis, which demonstrated that calibration data of individual curves were normally distributed ($p > 0.05$ WGhs), whilst

Table 2
Test statistics for colorimetric silica analysis in different calibration matrices. S: external standard curve, M1 to M5: standard addition to membrane fouling extracts from five membrane samples with different foulant characteristics. Raw data: all calibration measurements (triplicates per concentration) were considered in the analysis. Means: only the mean values were considered for each calibration point (1 point per concentration)

(a)   Values of statistical parameters of individual regression lines

Dataset	Statistical test	Calibration matrix					
		S	M1	M2	M3	M4	M5
Raw	Outlier detected in Grubbs test	None	None	None	None	None	None
	Shapiro–Wilk p	0.22	0.10	0.13	0.10	0.28	0.10
	White p	0.97	0.30	0.49	0.95	0.97	0.92
	R^2	0.99	1.00	1.00	1.00	0.99	1.00
	Regression p	3.2×10^{-13}	5.0×10^{-12}	1.3×10^{-12}	3.9×10^{-13}	2.8×10^{-10}	2.7×10^{-13}
Means	Outlier detected in Grubbs test	None	None	None	None	None	None
	Shapiro–Wilk p	0.28	0.45	0.46	0.46	0.62	0.45
	R^2	0.99	1.00	1.00	1.00	0.99	1.00
	Regression p	5.3×10^{-5}	5.1×10^{-6}	2.2×10^{-6}	1.6×10^{-6}	3.9×10^{-6}	9.1×10^{-7}

(b)   Pairwise analysis of slopes of calibration lines. S: external standard curve, M1 to M5: standard addition to membrane fouling extracts from five membrane samples with different foulant characteristics. Student t analysis performed with unspooled standard error. WGhs: within groups heteroscedasticity by the Breusch–Pagan test; BGhs: between groups heteroscedasticity by the Breusch–Pagan test

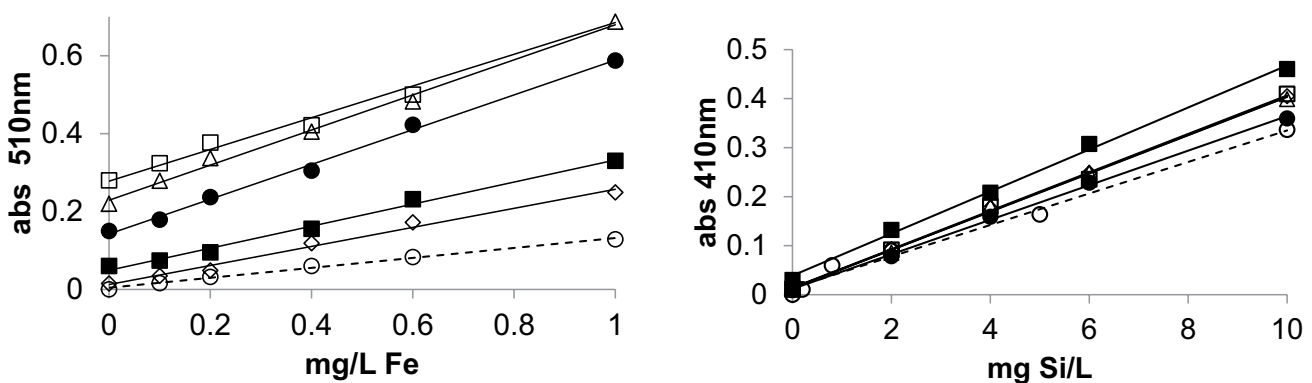| Dataset	Test parameter	S/M1	S/M2	S/M3	S/M4	S/M5
Raw	Student t p	0.01	0.00	0.00	0.02	0.18
	WB	0.17	0.13	0.12	0.20	0.55
	WGhs	0.72	0.91	0.86	0.39	0.56
	BGhs	0.80	0.81	0.50	0.06	0.28
Means	Student t p	0.13	0.07	0.06	0.21	0.58

Fig. 5. Calibration curves in colorimetric assays for silica and total iron. Each data point represents the average of three independent measurements, standard deviations were always within the size of the dots. External standard calibration: open dots. Standard addition calibrations in sample M1 (open squares), M2 (triangles), M3 (diamonds), M4 (filled squares), M5 (filled dots).

the different combinations of external and matrix additions datasets were all non-normally distributed (pBGhs < 0.05, when calibration slopes of standard addition and external calibration are statistically similar, the combined calibrations data should follow a normal (homoscedastic) distribution). Colorimetric iron quantification in membrane foulant extracts, therefore, needs to be performed by standard addition. The assay, however, worked well in all sample matrices, since absorption at 410 nm was directly proportional to added analyte.

For silica, there was a marked difference in outcomes of statistical comparisons of external standard and standard addition calibrations. In the Student-t test, 4 out of 5 slope pairs were statistically different, but the slopes of all five pairs were statistically similar according to the WB statistics (Table 2). The combined calibration datasets were also tested for heteroscedasticity, for example, for non-normal distribution of datapoints. Both individual calibration curve data ($p > 0.05$ WGhs) as well as combined calibration datasets were normally distributed (pBGhs < 0.05), a prerequisite for application of the Student t comparison (Table 2). Andrade and Estévez-Pérez [23] in their detailed discussion of advantages and disadvantages of different methods for the statistical comparisons of calibration slopes concluded that the Student t-test based on the standard error of regression models must be used in a typical laboratory calibration setting with a relatively small number of samples (<20) per calibration curve. Estévez-Pérez et al. [24] in a study on the application of bootstrap methods for calibration curve slope comparison concluded that the Student t-test was superior to bootstrap methods in situations where calibration data are normally distributed as demonstrated by the homoscedastic distribution of silica calibration data. Therefore, we recommend standard addition for colorimetric silica analysis as well. Silica analysis of fouled membranes by the colorimetric test employed in this study will only measure the silica species that react with aminomolybdate, the reactive silica [21]. Reactive silica includes monomeric, dimeric and up to tetrameric silica molecules [55,56]. The amorphous polymerized silica deposit typical of membranes heavily impacted by silica [6,57] will not be quantitatively analyzed by the photometric technique. The carbonate digestion step that precedes the aminomolybdate reaction will only depolymerize colloidal silica particles but not the entire deposit [21].

Standard addition calibration is not popular amongst practitioners, since it is perceived as adding cost and complexity to the analytical procedure. The authors did not find a report discussing the need of standard addition calibration with the colorimetric silica analysis method. Most of the few reports describing standard addition in colorimetric iron analysis are directed at using this technique as a strategy to co-analyze other metals in the same sample [58,59]. Standard addition, originally conceived as a simple means to correct for matrix interferences, has since evolved into a rather complex technique [60]. Analytical interferences are commonly classified into two categories. Spectral or translational interferences are disturbances that impact directly the spectrum or other signal measured in analysis. These interferences are called translational because they generally result in a parallel displacement of the standard addition calibration curve relative to the external standard calibration line. Non-spectral interferences consist of undesired chemical reactions that change the concentrations of the target analytes or of the analytical reagents used in analysis. These interferences are also called rotational effects, because they tend to change the slope of the calibration curve. Interferences in both iron- and silica analysis were of the rotational type.

The first and most simple countermeasure to deal with these interferences is sample dilution, which has to be made such that the target analytes in the dilute sample still remain above the quantitation limit of the method. An alternative approach to deal with unspecified matrix interference is the H-point standard addition procedure proposed by Wieczorek et al. [61]. This method relies on the establishment of a set of three standard addition calibrations each one performed in a different chemical environment, for example, at three different pH values. The common intersect of the three calibration plots is the H-point and corresponds to the true value of the analyte. This procedure is relatively easy to implement in a laboratory setting with a specialized workforce, but very cumbersome to be executed in the field by technical staff inexperienced in analytical chemistry. Chemical analysis as part of a membrane autopsy performed in a production plant environment cannot be expected to produce an extensive list of chemically precise results, but it has to provide a clear indication of the main cause of membrane failure. Much critical information about the nature of the foulants is gained from visual inspection of the membrane, from careful evaluation of feed, product and reject water quality analysis reports and from critical review of plant performance data. Foulants can be effectively removed from the membrane sample in the field with a kitchen blender, which produces a solution ready for chemical analysis by field tests. External standard calibrations routinely incorporated into field analysis kits provide sufficient precision for such analyses. More accurate results would be required to test for effects after changes to the processing stream, for example, adjustments to pretreatment, where comparisons of data before and after the events are needed. In these instances, it will be important to know whether the field analytical procedure is prone or not to severe matrix interference, since the nature of the matrix may have changed after process adjustments. A simplified standard addition calibration check with two standard additions should be sufficient to identify potential matrix interferences. One of the concentrations should be as close as possible to the upper quantitation limit [60], the second one at half that value. The addition standards would have to be prepared in a laboratory, but could be easily dispensed in the field with pipettes or similar semi-automatic volumetric dispensers.

4. Conclusion

Membrane foulants were best removed by homogenization in a blender followed by gentle scraping, whilst sonication was ineffective. Even the best removal techniques left a residual thin fouling film on the membrane surface. 3 h of time were sufficient to allow for sample drying at 105°C. Loss-on-ignition at 550°C was completed after 20 min, but the significant reductions of $FeCl_3$ (50%), ammonium chloride and ammonium sulfate (both 100%) demonstrate that this technique may not be an accurate measure of organic

matter content in foulant samples containing inorganics. Colorimetric analysis of iron by the phenanthroline method and of silica by the ammonium molybdate method required standard addition calibration for correct quantification of the analytes. Fouling removal with a kitchen blender produced homogeneous extracts suitable for chemical analysis with field kits.

Acknowledgments

References

[1] IDA, International Desalination Yearbook 2017–2018, Media Analytics Ltd., Oxford, UK, 2017.

[2] Z. Liu, J. Cao, C. Li, H. Meng, A review on cleaning of nano-filtration and reverse osmosis membranes used for water treatment, Desal. Wat. Treat., 87 (2017) 27–67.

[3] S. Jiang, Y. Li, B.P. Ladewig, A review of reverse osmosis membrane fouling and control strategies, Sci. Total Environ., 595 (2017) 567–583.

[4] R.P. Schneider, L.M. Ferreira, P. Binder, J.R. Ramos, Analysis of foulant layer in all elements of an RO train, J. Membr. Sci., 261 (2005) 152–162.

[5] M. Shmulevsky, X. Li, H. Shemer, D. Hasson, R. Semiat, Analysis of the onset of calcium sulfate scaling on RO membranes, J. Membr. Sci., 524 (2017) 299–304.

[6] R.Y. Ning, Discussion of silica speciation, fouling, control and maximum reduction, Desalination, 151 (2003) 67–73.

[7] H.-C. Flemming, J. Wingender, U. Szewzyk, P. Steinberg, S.A. Rice, S. Kjelleberg, Biofilms: an emergent form of bacterial life, Nat. Rev. Microbiol., 14 (2016) 563–575.

[8] H.-C. Flemming, J. Wingender, The biofilm matrix, Nat. Rev. Microbiol., 8 (2010) 623–633.

[9] J.S. Vrouwenvelder, S.A. Manolarakis, J.P. van der Hoek, J.A.M. van Paassen, W.G.J. van der Meer, J.M.C. van Agtmaal, H.D.M. Prummel, J.C. Kruithof, M.C.M. van Loosdrecht, Quantitative biofouling diagnosis in full scale nanofiltration and reverse osmosis installations, Water Res., 42 (2008) 4856–4868.

[10] F. Leitz, Membrane Element Autopsy Manual, Water Treatment Technology Program Report No. 17, US Department of the Interior, Bureau of Reclamation, 1996.

[11] E.W.F. de Roever, I.H. Huisman, Microscopy as a tool for analysis of membrane failure and fouling, Desalination, 207 (2007) 35–44.

[12] M. Pontié, S. Rapenne, A. Thekkedath, J. Duchesne, V. Jacquemet, J. Leparc, H. Suty, Tools for membrane autopsies and antifouling strategies in seawater feeds: a review, Desalination, 181 (2005) 75–90.

[13] R.S. Pembrey, K.C. Marshall, R.P. Schneider, Cell Surface Analysis Techniques: What Do Cell Preparation Protocols Do to Cell Surface Properties?, Appl. Environ. Microbiol., 65 (1999) 2877–2894.

[14] R.P. Schneider, Comparative analysis of thermodynamic approaches and diagnostic liquids for determination of contact angle-derived physicochemical parameters of solids coated with conditioning films: A practioner's perspective, J. Adhes. Sci. Technol., 11 (1997) 65–93.

[15] P. Xu, C. Bellona, J.E. Drewes, Fouling of nanofiltration and reverse osmosis membranes during municipal wastewater reclamation: Membrane autopsy results from pilot-scale investigations, J. Membr. Sci., 353 (2010) 111–121.

[16] T. Tran, B. Bolto, S. Gray, M. Hoang, E. Ostarcevic, An autopsy study of a fouled reverse osmosis membrane element used in a brackish water treatment plant, Water Res., 41 (2007) 3915–3923.

[17] S.T.V. Sim, W.B. Krantz, T.H. Chong, A.G. Fane, Online monitor for the reverse osmosis spiral wound module — Development of the canary cell, Desalination, 368 (2015) 48–59.

[18] S. Jeong, G. Naidu, R. Vollprecht, T.O. Leiknes, S. Vigneswaran, In-depth analyses of organic matters in a full-scale seawater desalination plant and an autopsy of reverse osmosis membrane, Sep. Purif. Technol., 162 (2016) 171–179.

[19] K. Donegan, C. Matyac, R. Seidler, A. Porteous, Evaluation of methods for sampling, recovery, and enumeration of bacteria applied to the phylloplane, Appl. Environ. Microbiol., 57 (1991) 51–56.

[20] G.R. Bruce, P.S. Gill, Estimates of precision in a standard additions analysis, J. Chem. Educ., 76 (1999) 805–807.

[21] APHA, Standard Methods for the Examination of Water and Wastewater, 22nd Ed., American Public Health Association, Washington, DC, New York, 2012.

[22] C. Zaiontz, www.real-statistics.com, 2017.

[23] J.M. Andrade, M.G. Estévez-Pérez, Statistical comparison of the slopes of two regression lines: a tutorial, Anal. Chim. Acta, 838 (2014) 1–12.

[24] G. Estévez-Pérez, J.M. Andrade, R.R. Wilcox, Bootstrap approach to compare the slopes of two calibrations when few standards are available, Anal. Chem., 88 (2016) 2289–2295.

[25] Anon, https://www.r-project.org, 2016.

[26] H.-C. Flemming, G. Schaule, T. Griebe, J. Schmitt, A. Tamach-kiarowa, Biofouling the Achilles heel of membrane processes, Desalination, 113 (1997) 215–225.

[27] S. Kanazawa, S. Takeshima, K. Ohta, Effect of waring blender treatment on the counts of soil microorganisms, Soil Sci. Plant Nutr., 32 (1986) 81–89.

[28] E.M. Bejarano, R.P. Schneider, Use of fluorescent lectin probes for analysis of footprints from *Pseudomonas aeruginosa* MDC on hydrophilic and hydrophobic glass substrata, Appl. Environ. Microbiol., 70 (2004) 4356–4362.

[29] A. Siddiqui, S. Lehmann, Sz. S. Bucs, M. Fresquet, L. Fel, E.I.E.C. Prest, J. Ogier, C. Schellenberg, M.C.M. van Loosdrecht, J.C. Kruithof, J.S. Vrouwenvelder, Predicting the impact of feed spacer modification on biofouling by hydraulic characterization and biofouling studies in membrane fouling simulators, Water Res., 110 (2017) 281–287.

[30] H.M. Kyllönen, P. Pirkonen, M. Nyström, Membrane filtration enhanced by ultrasound: a review, Desalination, 181 (2005) 319–335.

[31] S. Muthukumaran, S.E. Kentish, G.W. Stevens, M. Ashokkumar, Application of ultrasound in membrane separation processes: a review, Rev. Chem. Eng., 22 (2006) 155–194.

[32] C. Gómez-Suárez, H.J. Busscher, H.C. van Der Mei, Analysis of bacterial detachment from substratum surfaces by the passage of air-liquid interfaces, Appl. Environ. Microbiol., 67 (2001) 2531–2537.

[33] A.J. Ansari, F.I. Hai, T. He, W.E. Price, L.D. Nghiem, Physical cleaning techniques to control fouling during the pre-concentration of high suspended-solid content solutions for resource recovery by forward osmosis, Desalination, 429 (2018) 134–14.

[34] X. Chai, T. Kobayashi, N. Fujii, Ultrasound-associated cleaning of polymeric membranes for water treatment, Sep. Purif. Technol., 15 (1999) 139–146.

[35] T. Kobayashi, X. Chai, N. Fujii, Ultrasound enhanced cross-flow membrane filtration, Sep. Purif. Technol., 17 (1999) 31–40.

[36] D. Feng, J.S.J. van Deventer, C. Aldrich, Ultrasonic defouling of reverse osmosis membranes used to treat wastewater effluents, Sep. Purif. Technol., 50 (2006) 318–323.

[37] J. Wang, X. Gao, Y. Xu, Q. Wang, Y. Zhang, X. Wang, C. Gao, Ultrasonic-assisted acid cleaning of nanofiltration membranes fouled by inorganic scales in arsenic-rich brackish water, Desalination, 377 (2016) 172–177.

[38] Y.-S. Li, L.-C. Shi, X.-F. Gao, J.-G. Huang, Cleaning effects of oxalic acid under ultrasound to the used reverse osmosis membranes with an online cleaning and monitoring system, Desalination, 390 (2016) 62–71.

[39] B. Garcia-Fayos, J.M. Arnal, A. Gimenez, S. Alvarez-Blanco, M. Sancho, Study of ultrasonically enhanced chemical cleaning

of SWRO membranes at pilot plant scale, Desal. Wat. Treat., 88 (2017) 1–7.

[40] D.G. Shchukin, E. Skorb, V. Belova, H. Möhwald, Ultrasonic Cavitation at Solid Surfaces, Adv. Mater., 23 (2011) 1922–1934.

[41] S. Broekman, O. Pohlmann, E.S. Beardwood, E. Cordemans de Meulenaer, Ultrasonic treatment for microbiological control of water systems, Ultrason. Sonochem., 17 (2010) 1041–1048.

[42] M. Herzberg, M. Elimelech, Physiology and genetic traits of reverse osmosis membrane biofilms: a case study with *Pseudomonas aeruginosa*, ISME J., 2 (2008) 180–194.

[43] M. Marroquin, A. Vu, T. Bruce, R. Powell, S.R. Wickramasinghe, S.M. Husson, Location and quantification of biological foulants in a wet membrane structure by cross-sectional confocal laser scanning microscopy, J. Membr. Sci., 453 (2014) 282–291.

[44] M. Marroquin, A. Vu, T. Bruce, S.R. Wickramasinghe, L. Zhao, S.M. Husson, Evaluation of fouling mechanisms in a symmetric microfiltration membrane using advanced imaging, J. Membr. Sci., 465 (2014) 1–13.

[45] H. Hagihara, K. Ito, N. Oshima, A. Yabuuchi, H. Suda, H. Yanagishita, Depth profiling of the free-volume holes in cellulose triacetate hollow-fiber membranes for reverse osmosis by means of variable-energy positron annihilation lifetime spectroscopy, Desalination, 344 (2014) 86–89.

[46] T. Fujioka, N. Oshima, R. Suzuki, W.E. Price, L.D. Nghiem, Probing the internal structure of reverse osmosis membranes by positron annihilation spectroscopy: gaining more insight into the transport of water and small solutes, J. Membr. Sci., 486 (2015) 106–118.

[47] A.S. Gorzalski, O. Coronell, Fouling of nanofiltration membranes in full- and bench-scale systems treating groundwater containing silica, J. Membr. Sci., 468 (2014) 349–359.

[48] K.C. Marshall, R. Pembrey, R.P. Schneider, The relevance of X-ray photoelectron spectroscopy for analysis of microbial cell surfaces: a critical review, Colloids Surf., B, 2 (1994) 371–376.

[49] J. Vaxelaire, P. Cézac, Moisture distribution in activated sludges: a review, Water Res., 38 (2004) 2215–2230.

[50] E. Yildirim, Y. Zhang, J.L. Lutkenhaus, M. Sammalkorpi, Thermal transitions in polyelectrolyte assemblies occur via a dehydration mechanism, ACS Macro Lett., 4 (2015) 1017–1021.

[51] F.M. Etzler, W. Drost-Hansen, A Role of Water in Growth, Metabolism and Intracellular Organization, M. Blank, Ed., Advances in Chemistry 188, Bioelectrochemistry: Ions, Surfaces, Membranes, American Chemical Society, Columbus, Ohio, 1980, pp. 485–497.

[52] W. Deng, X. Li, J. Yan, F. Wang, Y. Chi, K. Cen, Moisture distribution in sludges based on different testing methods, J. Environ. Sci., 23 (2011) 875–880.

[53] J.G. Speight, Lange's Handbook of Chemistry, 16th Ed., McGraw-Hill, Toronto, 2004.

[54] L. Erdey, S. Gál, G. Liptay, Thermoanalytical properties of analytical-grade reagents: ammonium salts, Talanta, 11 (1964) 913–940.

[55] G.B. Alexander, The reaction of low molecular weight silicic acids with molybdic acid, J. Am. Chem. Soc., 75 (1953) 2887–2888.

[56] M. Tanaka, K. Takahashi, Silicate species in high pH solution molybdate, whose silica concentration is determined by colorimetry, Anal. Chim. Acta, 429 (2001) 117–123.

[57] B. Mi, M. Elimelech, Silica scaling and scaling reversibility in forward osmosis, Desalination, 312 (2013) 75–81.

[58] H. Abdollahi, Simultaneous spectrophotometric determination of chromium(VI) and iron(III) with chromogenic mixed reagents by H-point standard addition method and partial least squares regression, Anal. Chim. Acta, 442 (2001) 327–336.

[59] A. Safavi, H. Abdollahi, Application of the H-point standard addition method to the speciation of Fe(II) and Fe(III) with chromogenic mixed reagents, Talanta, 54 (2001) 727–734.

[60] J.E.T. Andersen, The standard addition method revisited, TrAC, Trends Anal. Chem., 89 (2017) 21–33.

[61] M. Wieczorek, S. Rengevicova, P. Świt, A. Woźniakiewicz, J. Kozak, P. Kościelniak, New approach to H-point standard addition method for detection and elimination of unspecific interferences in samples with unknown matrix, Talanta, 170 (2017) 165–172.
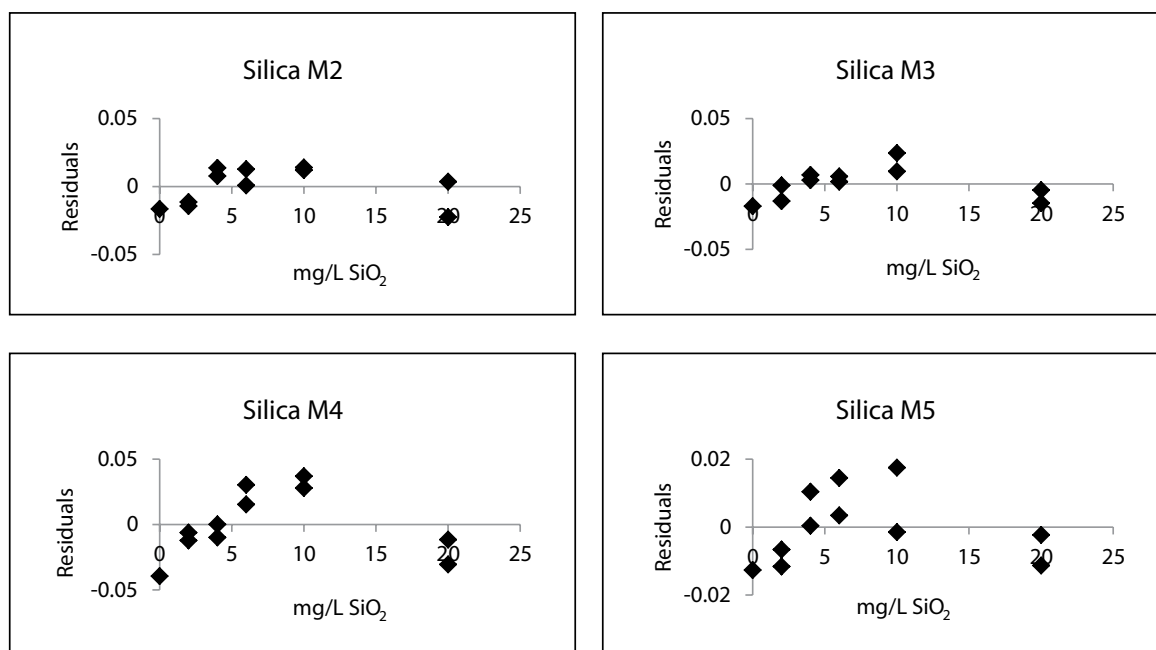
Supplementary Information

Fig. S1. Plot of residuals for colorimetric determination of silica.
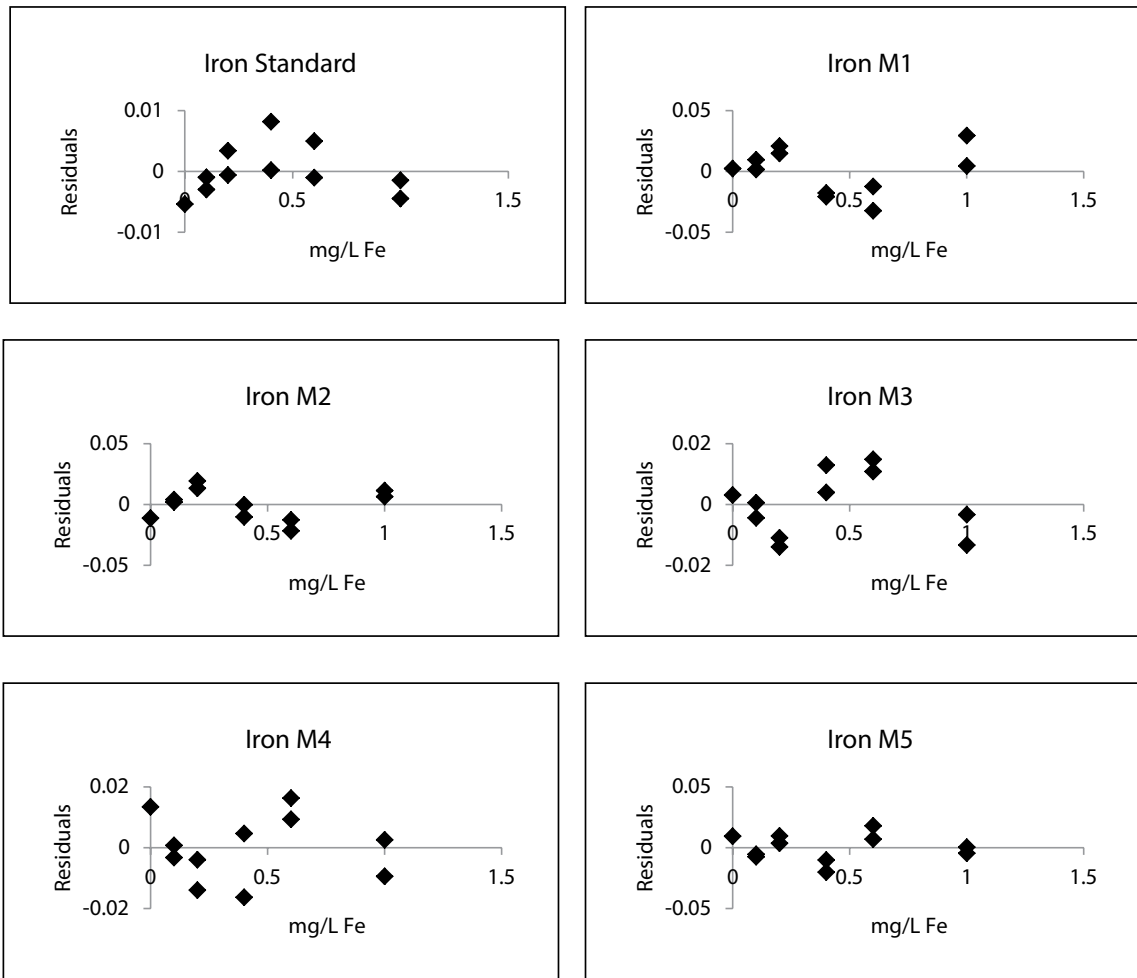
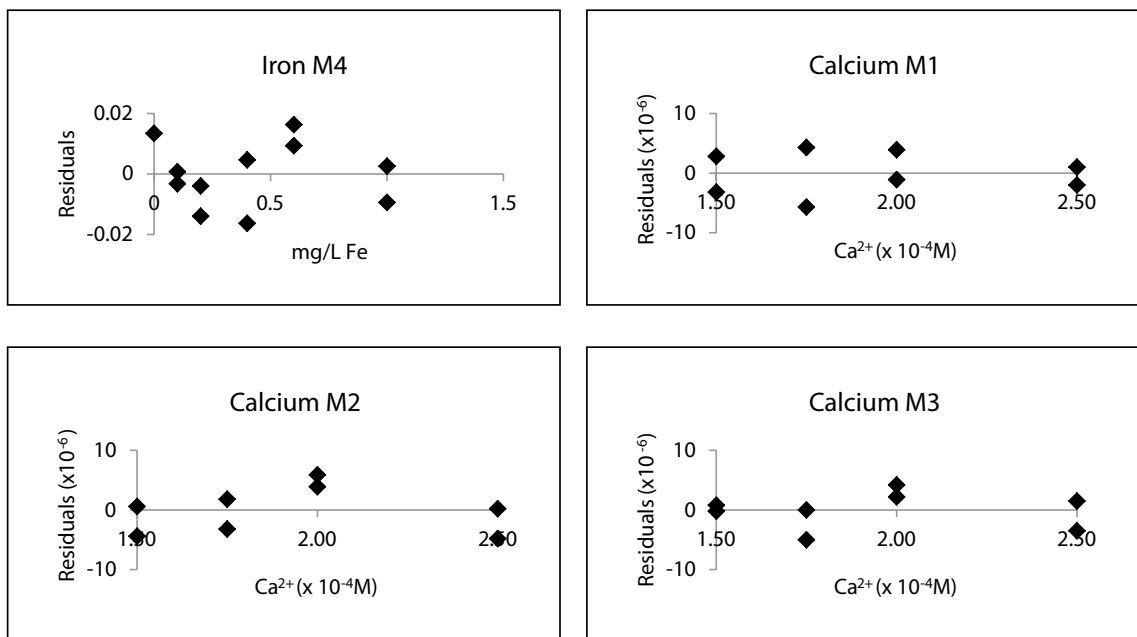Fig. S2. Plot of residuals for colorimetric determination of iron.
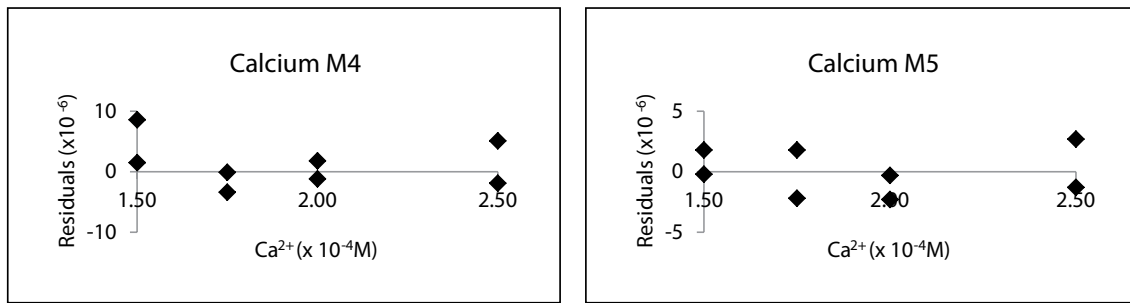

Fig. S3. Continued

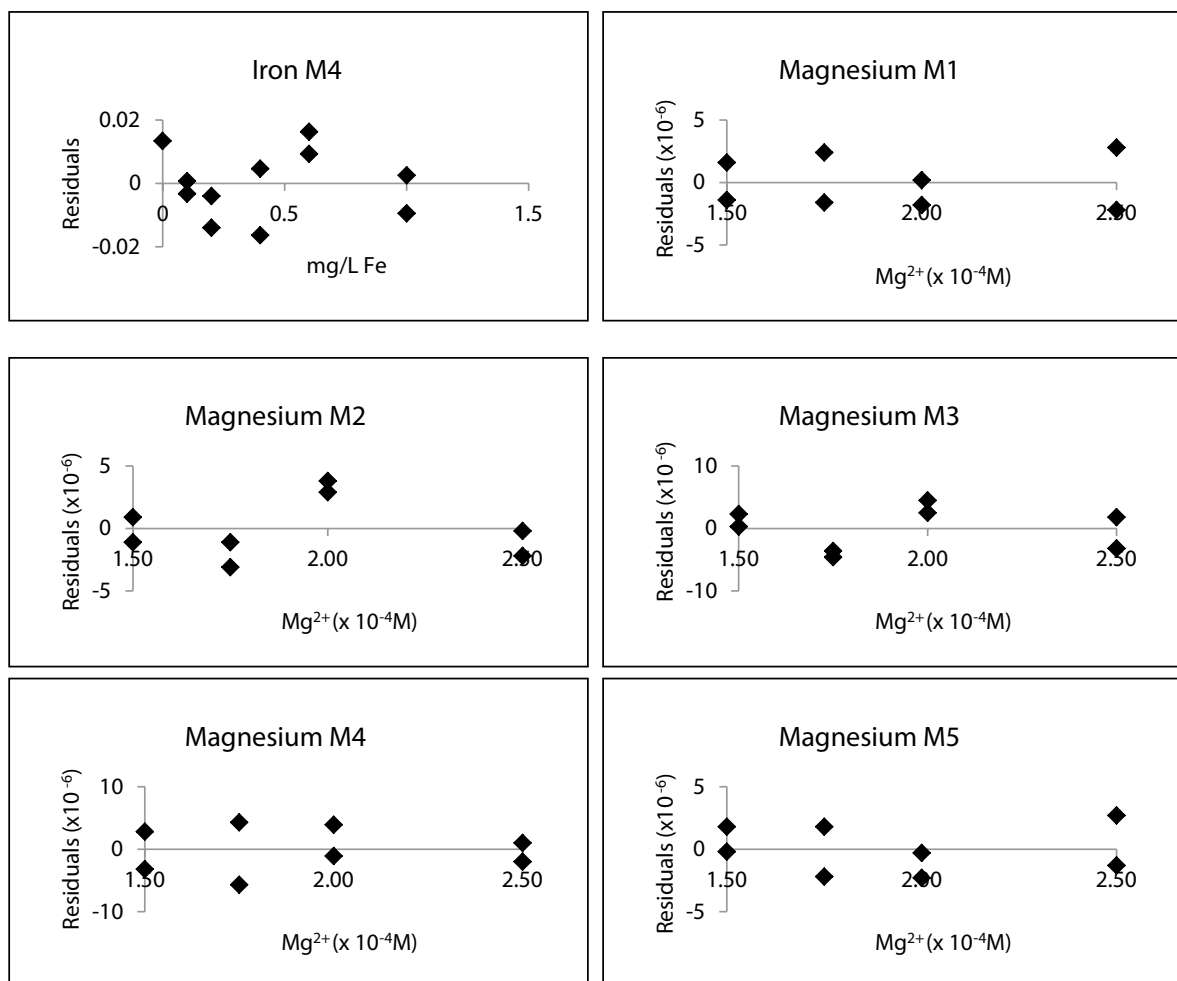Fig. S3. Plot of residuals for colorimetric determination of calcium.

Fig. S4. Plot of residuals for colorimetric determination of magnesium.